

HYBRID ROCKET HOT-GAS DRIVER FOR DIRECT-CONNECT SCRAMJET THERMO-STRUCTURAL SCREENING

Alison Roco[1], Harry Chisholm[2] & David Hartley[1]

[1]Defence Science and Technology Group
[2]Advanced Composite Structures Australia

Abstract

Despite advances in scramjet materials, simulations, and test capabilities, a lack of representative thermo-structural ground testing remains a barrier to the development of engine structures, particularly where long duration, high enthalpy test facilities are difficult to access. This work evaluates a direct-connect testing approach that uses a commercially available hybrid rocket engine as a hot-gas driver for thermo-structural assessment of a canonical Mach 6–8 carbon/carbon (C/C) scramjet combustor and nozzle. Two 30 s hot-fire tests were conducted under nominal and fuel lean operating conditions. Temperature and static wall pressure were measured directly and assessed against Reynolds-averaged Navier–Stokes (RANS) simulations, which provided derived flow quantities, including combustor entrance Mach number and predicted wall heat flux. Simulated static wall pressures ranged 57–295 kPa, peak predicted wall heat flux reached 5.1–7.1 MW/m^2, and combustor entrance Mach numbers were 2.4–2.5. The static wall pressures overlap the ranges reported for the HyShot 2 flight and HIFiRE direct-connect rig (HDCR) ground tests, while extending the test time relative to the reference cases. The combustor entrance Mach numbers span the HyShot 2 value of 2.4 and sit just below the HDCR facility nozzle exit value of 2.55. The method therefore provides an intermediate fidelity screening step for combustor and nozzle structures, prior to higher fidelity combustion and flight testing. Species mismatch is the principal fidelity limitation.

Keywords: scramjet, direct-connect testing, thermo-structural testing, hybrid rocket engine, carbon/carbon composites

1. Introduction

Scramjet combustors and nozzles operate in severe coupled aerothermal and chemical environments. At Mach 6–8 flight conditions, wall heat fluxes can range 0.6–7 MW/m^2, while local temperatures can exceed the upper temperature limits of advanced thermal management materials [1, 2]. Carbon/carbon (C/C), and other typical candidate refractory materials for use in scramjets, can exhibit strongly environment dependent behaviour because their thermal response, oxidation, ablation, and mechanical degradation depend jointly on heat flux, pressure, flow speed, chemical species, duration of heat exposure, and manufacturing details [3–5]. Representative thermo-structural testing is therefore required before flight to assess whether engine structures can survive realistic aerothermal loads.

1.1 Scramjet Thermo-structural Testing

No single ground test method reproduces all relevant scramjet flight conditions, and each compromises on a different parameter. Impulse facilities can reproduce high enthalpy, high speed flow conditions and are valuable for flow physics studies, but their test durations of microseconds to milliseconds are too short for transient through-thickness heating, material recession, and other transient thermo-structural effects to develop [6–10]. Unit and coupon tests, including those that use

oxy-acetylene torches, plasma facilities, and radiative heaters, and other material screening methods can produce controlled thermal loading and long exposure times but do not reproduce the coupled internal flow environment of a scramjet combustor and nozzle, including shock wave/boundary layer interactions (SWBLIs) and representative pressures [11–14]. Direct-connect tests provide a higher fidelity assessment of engine structures because they can reproduce internal flow path Mach number, pressure, enthalpy, shock structure, and combustion related loading, while not requiring a full inlet or flight vehicle [15–19]. For direct-connect tests the compromise is access rather than physics.

Direct-connect facilities are limited, especially for early stage structural development and repeated subscale or component level testing. This limitation is particularly relevant for countries without access to large international scramjet test facilities. Australia, for example, has scramjet flight heritage and impulse test capability, but not routine domestic access to the long duration combustion heated or arc heated facilities typically used for scramjet durability testing [6, 20–22]. Reliance on major facilities also slows iteration, and flight testing is too expensive and difficult to be the first check of structural survivability. A more accessible intermediate screening method is therefore useful before international facility access or flight testing.

A hybrid rocket engine can act as a compact hot-gas driver for a direct-connect structural test. Rocket engines generate high temperature, high speed exhausts that can be expanded into a scramjet test article, providing long duration aerothermal loads. The chemistry is not equivalent to an air breathing engine because the hybrid rocket exhaust is dominated by H_2O and CO_2, whereas hydrocarbon scramjet combustion products are dominated by N_2. For thermo-structural screening rather than combustion performance assessment, however, the method reproduces several dominant loading parameters, such as wall heat flux, static wall pressure, internal shock structure, SWBLI positions, flow speed, scale, and exposure duration.

1.2 Scope of this Work

This paper assesses whether a hybrid rocket engine can serve as an intermediate fidelity hot-gas driver for direct-connect thermo-structural screening of scramjet combustor and nozzle hardware. The method is not proposed as a replacement for chemically representative combustion testing or flight testing. The intended role is earlier in the test campaign, alongside impulse facility testing and before flight testing. The test campaign and numerical workflow reported here are documented in full in the first author's honours thesis [23].

2. Methods

2.1 Test Configuration

A direct-connect test was conducted using a commercially available hybrid rocket engine as the hot-gas driver for a Mach 6–8 canonical scramjet combustor and nozzle test article. The test article consisted of two cylindrical combustor modules and a conical nozzle module, each comprising a custom C/C liner supported by an external steel structure. The hybrid rocket nozzle was bolted directly to the scramjet combustor module entrance so that the supersonic rocket exhaust expanded through the full test article flow path. A schematic of the test arrangement is shown in Figure 1 and the internal module dimensions are shown in Figure 2. The assembled test configuration is shown in Figure 3.

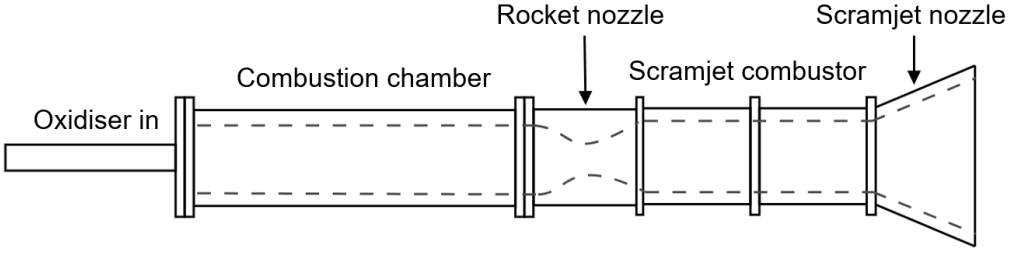


Figure 1 – High level schematic of the hybrid rocket engine directly connected to the scramjet test article.

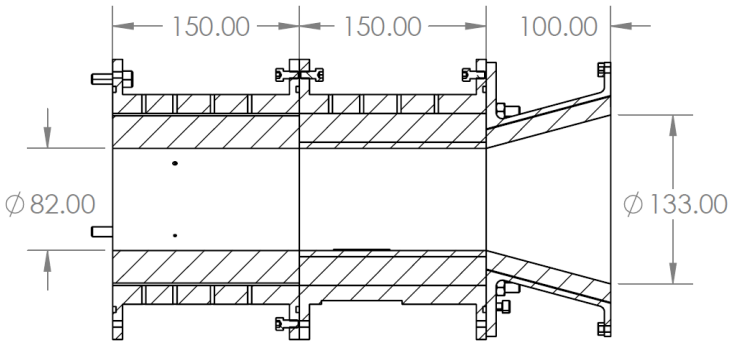


Figure 2 – Cross section of the combustor and nozzle with internal dimensions in mm.

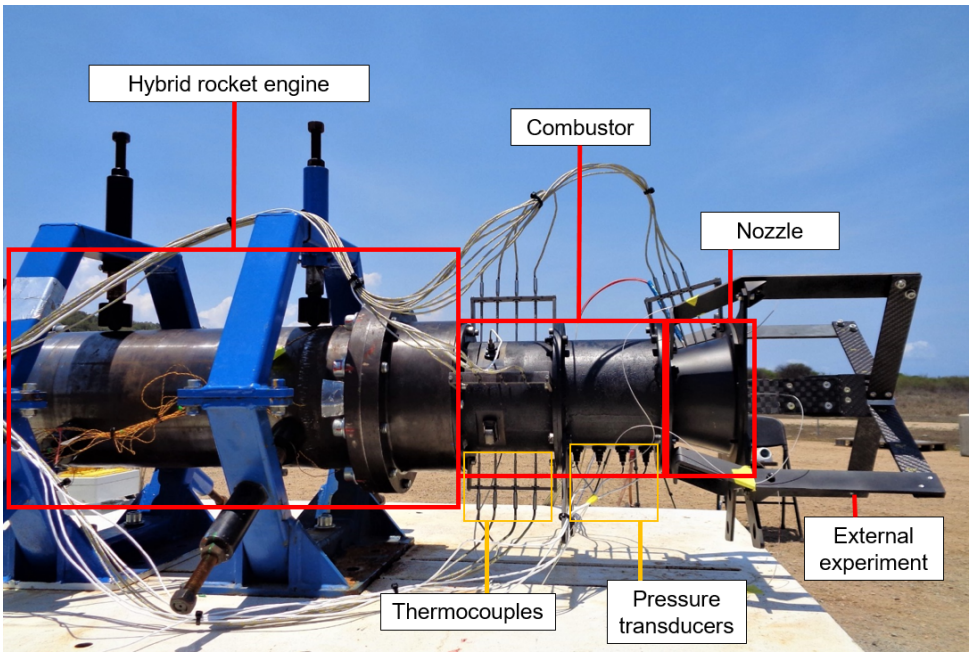


Figure 3 – Hybrid rocket engine directly connected to the scramjet test article showing instrumentation.

2.2 Operating Conditions

Two 30 s hot-fire tests were conducted under nominal and fuel lean hybrid rocket operating conditions. Each test followed a short priming pulse used to verify stable rocket operation before the sustained firing. The tests were conducted on consecutive days with ambient temperatures of 28–32°C (301–305 K) at sea level pressure. The nominal case used an oxidiser-to-fuel ratio of O/F = 7 and the lean case used O/F = 8.5. At 15 s into the sustained firing, the hybrid rocket nozzle exit temperature was approximately $T_e \approx$ 1750–1880 K and the nozzle exit pressure was approximately $P_e \approx$ 0.163–0.170 MPa. Table 1 summarises the nozzle throat and exit conditions at 30 s.

Table 1 – Nominal and lean hybrid engine conditions at $t = 30$ s for the rocket nozzle throat (t) and exit (e) planes.

Parameter	Units	Nominal	Lean
T_t	K	2475	2479
T_e	K	1748	1877
P_t	MPa	1.54	1.34
P_e	MPa	0.150	0.136

The hybrid rocket engine used hydrogen peroxide as an oxidiser and a solid fuel motor to produce

combustion products that were partially representative of a hydrocarbon fuelled air breathing engine. The fuel lean condition was used to assess sensitivity to changed exhaust composition and increased oxidising species content. At the hybrid rocket nozzle exit, the nominal case was 63.0% H_2O and 31.7% CO_2 by mass. The lean case contained higher H_2O and CO_2 mass fractions of 65.8% and 33.0%, respectively, with trace O_2 and OH. These exhaust compositions were relevant to C/C oxidation and erosion assessment but they were not chemically representative of scramjet combustion products that are dominated by N_2. The calculated nozzle exit species mass fractions are listed in Table 2.

Table 2 – Species mass fractions at the hybrid nozzle exit at $t = 15$ s.

Species	Nominal	Lean
CO	0.048	0.000
CO_2	0.317	0.330
H_2	0.005	0.000
H_2O	0.630	0.658
O_2	0.000	0.011
OH	0.000	0.001

2.3 Instrumentation and Data Acquisition

Wall temperature and static wall pressure were the primary measurements used to assess the test environment and validate the numerical workflow because they were measured directly. Mach number, wall heat flux, near-wall flow temperature, and shock structure are derived quantities obtained from the numerical simulations that were assessed against the measured pressure and temperature trends.

Type K thermocouples were embedded at multiple axial locations and depths within the combustor and nozzle liners. Readings above approximately 1500 K fall outside their reliable range and are treated as indicative only. Static wall pressure was measured using high-temperature Kulite XTEL-190 pressure transducers installed along the combustor wall. Pressure measurements were not taken in the nozzle module due to space and geometry constraints imposed by the nozzle material screening campaign. A load cell measured thrust from the hybrid rocket engine and infrared and optical cameras were used for flow visualisation and post-test forensic assessment. Post-test internal profiles were measured using a Hexagon Explorer 08.10.06 coordinate measuring machine (CMM) to quantify wall recession, reported as a circumferential average at each axial station. The sensor layout for the test article is shown in Figure 4.

Measurement uncertainty was separated into direct measurement uncertainty and modelling uncertainty. Direct measurement uncertainties are reported in Table 3. These values account for sensor tolerance, measurement noise, and uncertainty. Derived quantities, such as wall heat flux and Mach number, additionally depend on modelling assumptions, which include frozen chemistry, constant Prandtl number, steady-state inflow conditions, material properties, axisymmetric flow, and no geometry change during firing.

Table 3 – Representative measurement uncertainties used in data reduction.

Test Parameter	Uncertainty	Dominant Source
Temperature	0.75%	Sensor tolerance, operating range
Static wall pressure	0.5%	Sensor tolerance, noise
Thrust	4.1% nominal, 5.4% lean	Sensor tolerance, noise
Liner wall erosion	2.5%	CMM tolerance, measurement standard error

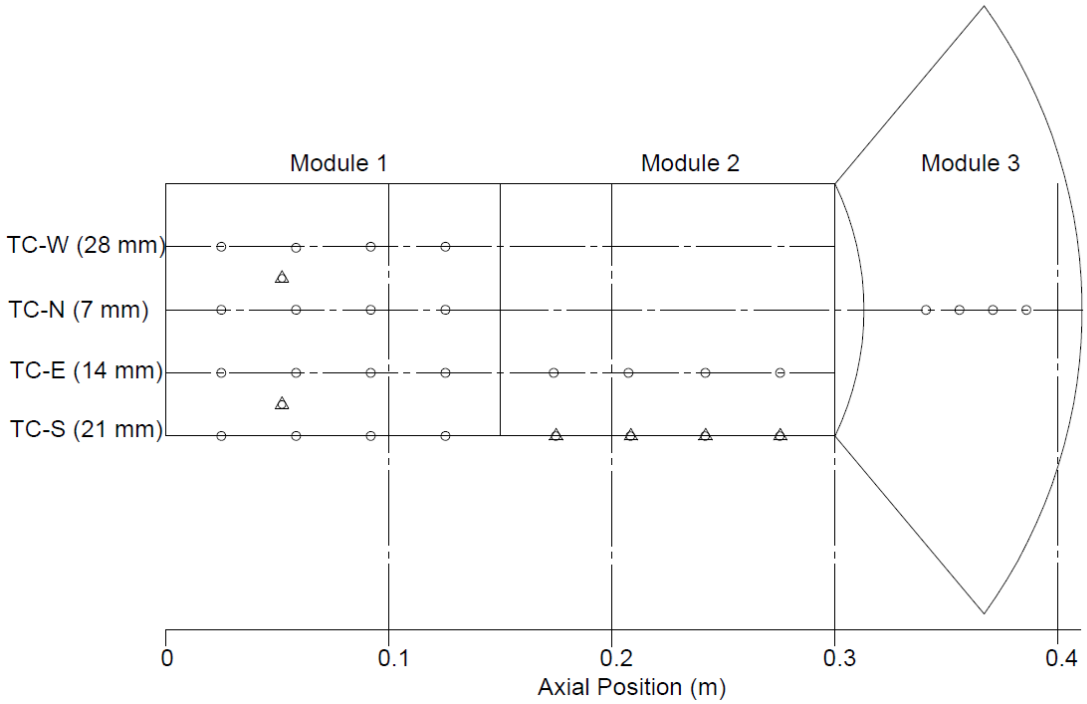


Figure 4 – Sensor layout for the direct-connect scramjet test article, shown as a flattened axial schematic. Static pressure transducers (△) and embedded thermocouples (o) are positioned along the combustor wall. Thermocouples (TC-N/E/S/W) are placed at multiple depths, measured relative to the internal engine liner wall.

2.4 Numerical Methods

Reynolds-averaged Navier–Stokes (RANS) simulations were performed using the open source solver Eilmer4 to model the internal flow from the hybrid rocket nozzle through the scramjet combustor and nozzle. The computational domain included the hybrid rocket nozzle, from the throat to the exit plane, and the full internal scramjet test article flow path, as shown in Figure 5. A structured mesh was generated with near-wall clustering to better resolve boundary layer effects and shock wave interaction with the walls.



Figure 5 – Computational domain used for the hybrid rocket nozzle and scramjet test article flow field simulation.

The simulations used the steady-state solver with second-order spatial accuracy and the Spalart–Allmaras–Edwards turbulence model. The inflow state was based on the calculated hybrid rocket throat conditions at 15 s and 30 s, with the flow assumed choked at the nozzle throat. The gas mixture was modelled using the calculated frozen species composition at the hybrid rocket nozzle exit at 15 s, at which point reactions were assumed to have ceased. The wall temperature was set at 300 K to allow wall heat flux to be estimated for subsequent thermal analysis. Major modelling assumptions and their possible implications are summarised in Table 4.

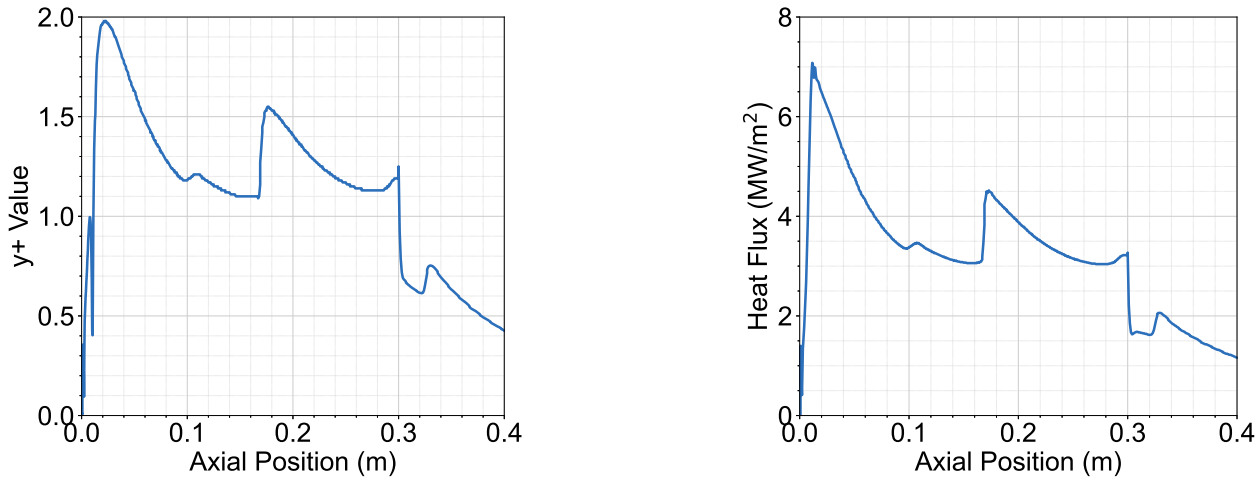
Table 4 – Modelling assumptions used in the flow simulations.

Assumption	Implication for interpretation
Rocket nozzle geometry was held constant for the 15 s and 30 s cases using the pre-test and post-test nozzle profiles, respectively.	Any progressive nozzle erosion between 0 s, 15 s, and 30 s was not captured, so gradual changes in mass flow rate, thrust, or shock position caused by throat and profile recession were not modelled.
The rocket exhaust was treated as axisymmetric.	Any swirl, asymmetric plume structures, or circumferential variations in shock impingement were not modelled.
The flow was treated as frozen and non-reacting downstream of the rocket nozzle.	Chemical reactions, afterburning, and changing species concentrations through the combustor and nozzle were not modelled.
Wall temperature was held constant in the flow solution.	Predicted wall heat flux is conservative where the real wall temperature increased during firing, since increasing wall temperature reduces the local gas to wall temperature difference.
The flow was solved as a steady-state condition at the 15 s and 30 s operating points.	Time-dependent changes in chamber pressure, nozzle geometry, mass flow rate, and shock motion were not modelled.
The simulation used the Spalart–Allmaras–Edwards turbulence model.	This turbulence model, and other RANS turbulence models, can overpredict local heat flux in high pressure regions and across steep pressure gradients, such as those encountered in SWBLIs.
The gas mixture was defined using calculated rocket nozzle exit species.	Any changes in gas mixture due to uneven burning or fuel formulation changes were not modelled.

The computational fluid dynamics (CFD) results were coupled to a transient thermal finite element model of the composite liner. The near-wall flow temperature and film coefficient were applied as boundary conditions to the liner model and a 30 s transient thermal analysis was performed to obtain a through-thickness temperature profile using Ansys Mechanical Finite Element Analysis software. The composite material was represented using a layered-shell mesh arrangement generated by the Ansys ACP-Pre toolbox.

Temperature dependent material properties of the C/C, including specific heat at constant pressure and thermal conductivity, were obtained through thermophysical material characterisation. The thermal model predicted the through-thickness wall temperature response for comparison with embedded thermocouple measurements. Wall heat flux is reported as a quantity derived from the validated RANS simulations, not as a direct measurement.

Grid convergence was assessed using Mach number and thrust as the monitored quantities. A grid convergence study showed monotonic thrust convergence, with the finest grid solution having a total thrust of 5.545 kN and an estimated numerical error of approximately 0.69%. The wall resolution parameter y^+ was minimised using clustered cells because predicted heat flux is sensitive to near-wall resolution, particularly near SWBLIs. The y^+ and wall heat flux from the nominal fuel condition RANS simulations are shown in Figures 6a and 6b, respectively.



(a) The y^+ value along the wall.

(b) The heat flux along the wall.

Figure 6 – The y^+ values and heat flux along the wall for the nominal simulation.

3. Results

3.1 Simulated Flow Path

The simulated flow field contained a repeating shock train through the combustor flow path for both operating conditions. Mach number and static pressure contours are shown in Figure 7. The nominal case produced slightly higher simulated Mach numbers and static wall pressures than the lean case. The combustor entrance Mach number was approximately 2.4–2.5 for both cases. Static wall pressure ranged 66–295 kPa for the nominal case and 57–250 kPa for the lean case.

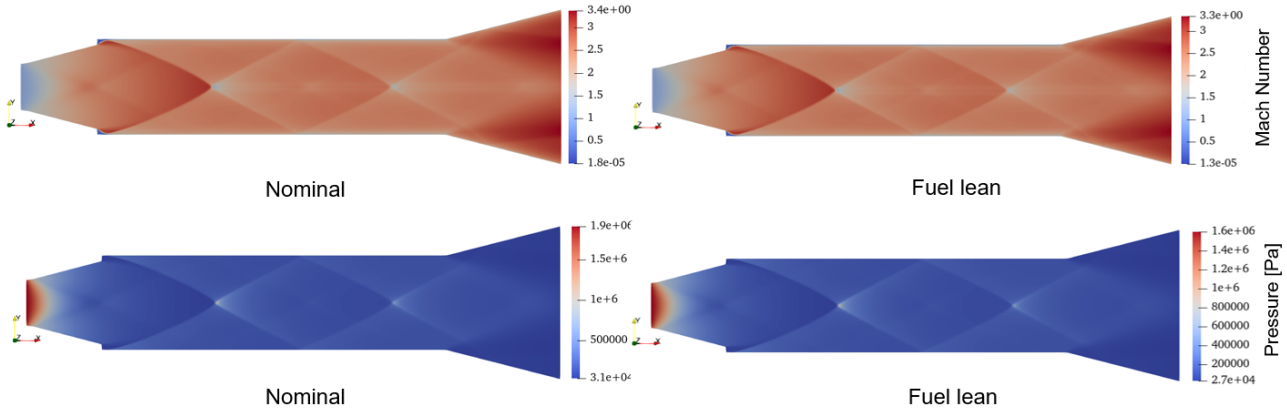


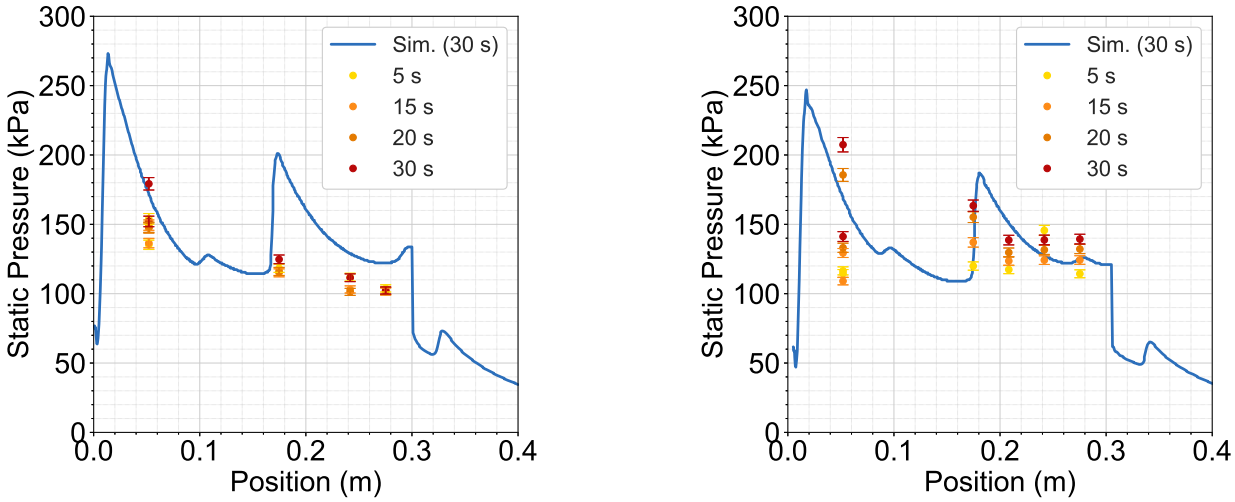
Figure 7 – Mach number (top) and pressure (bottom) contour plots for the nominal and fuel lean conditions at 30 s.

The simulated shock pattern is useful in interpreting the results because shock impingement and SWBLIs can produce local increases in wall pressure, near-wall temperature, and wall heat flux. These local effects are important for thermo-structural screening because they can cause non-uniform heating and accelerate material recession.

3.2 Simulation Validation Against Measured Pressure, Temperature, and Erosion Trends

Figure 8 compares simulated static wall pressure with measured static wall pressure at multiple times during the nominal and lean firings. The simulation curve corresponds to the steady-state 30 s operating condition, while the experimental traces show the temporal development of the measured wall pressure during firing. Measurement points were selected over a 1 s interval from each pressure trace after applying a Savitzky–Golay filter to the data.

The greatest variation in the pressure measurements is seen near regions where strong shocks are predicted, particularly for the lean case. In these regions, any asymmetry in the flow or axial



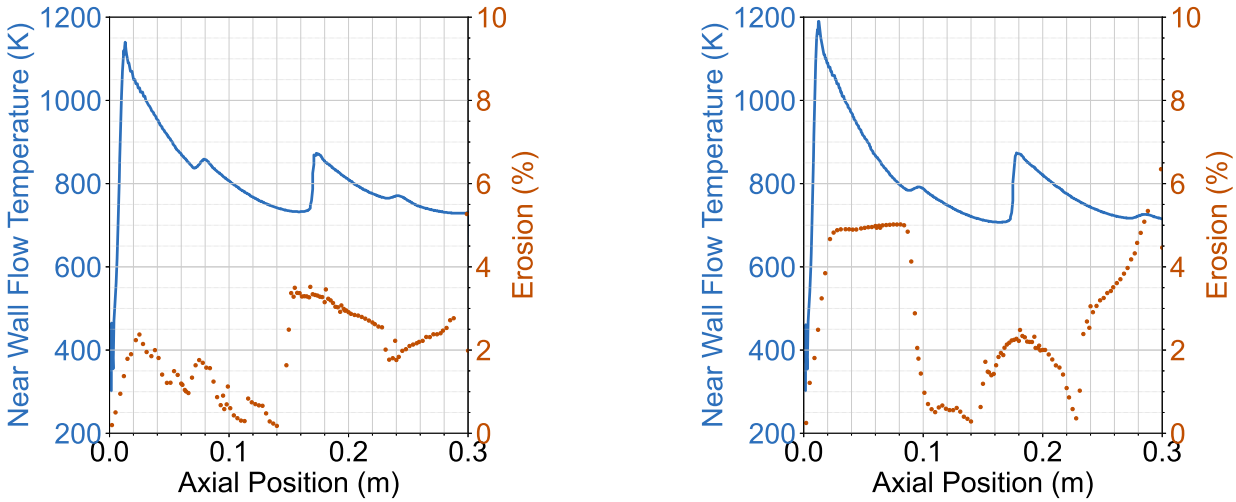
(a) Nominal condition test data.

(b) Lean condition test data.

Figure 8 – Static wall pressure measurements compared with CFD predictions for the combustor segment (Modules 1 and 2). The pressure transducer uncertainty was approximately 0.5%.

movement of the shock during the firing produces a large change in the pressure recorded at a fixed tap, because the pressure gradient across a shock is steep. Away from these areas, the simulated pressure more closely aligns with the measured static pressure.

Post-test wall recession measurements were compared with simulated near-wall flow temperature and predicted regions of shock impingement. Figure 9 shows that local erosion peaks broadly aligned with regions of elevated simulated near-wall temperature and shock wave/wall interaction, providing qualitative support for the predicted shock structure. Absolute erosion percentages cannot be interpreted quantitatively because material configuration varied between modules and particulate in the hybrid rocket exhaust may have contributed to mechanical recession mechanisms.

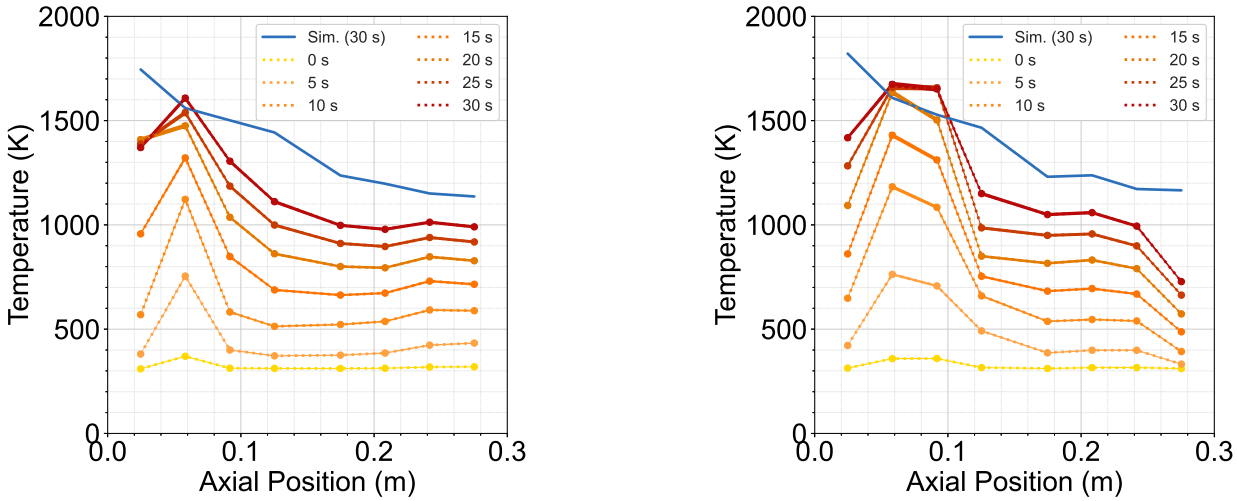


(a) Nominal condition test data.

(b) Lean condition test data.

Figure 9 – Simulated near-wall flow temperature at 30 s compared with post-test measured wall erosion for the combustor segment (Modules 1 and 2).

Figure 10 compares the predicted 30 s wall temperature from the transient thermal simulations to measured wall temperatures from the 7 mm (TC-N) thermocouples at selected times.



(a) Nominal condition test data.

(b) Lean condition test data.

Figure 10 – Experimental wall temperature measurements compared with temperature predictions for the combustor segment (Modules 1 and 2). The thermocouple reliable temperature measurement limit is approximately 1500 K.

It is worth noting that the largest disagreement between the measured and predicted temperature occurs in the same region where the first and strongest shock impinges on the wall. One possibility that may explain this disagreement is that erosion near those thermocouples leaves them closer to the flow than is modelled in the transient thermal simulation. Furthermore, the turbulence model is likely to overpredict the heat flux in regions where there are strong SWBLIs, leading to a higher temperature prediction in the thermal model.

Overall, the simulations reproduced the dominant pressure and temperature trends, and aligned with the shock structure implied by erosion measurements. The greatest modelling uncertainty appears to be near strong SWBLIs, where large measured pressure fluctuations occur and the turbulence model and wall temperature assumption can affect the predicted heating. Agreement was closer for the nominal condition than for the fuel lean condition. For the lean condition, the simulated shock positions did not match those implied by the measured pressure, temperature, and wall erosion. Test fidelity is therefore assessed against the nominal case, and the lean quantities are reported for comparison only.

3.3 Comparison with HyShot 2 and HIFiRE-2 Reference Data

The nominal and lean test conditions were compared with published HyShot 2 and Hypersonic International Flight Research Experimentation (HIFiRE) Flight 2 reference data to assess whether the hybrid rocket direct-connect method reproduced structurally relevant ranges of the flow and exposure conditions, as summarised in Table 5. HyShot 2 provides a hydrogen fuelled flight reference at Mach 7.75–8 [24], while HIFiRE-2 provides hydrocarbon fuelled flight and HIFiRE direct-connect rig (HDCR) ground test references. The comparison is not intended to imply equivalence in combustion physics or chemical environment.

The 30 s hybrid rocket firings provided longer-duration exposure than the flight test and ground test durations considered. For thermo-structural screening, a longer test duration allows wall heating and material responses to fully develop, which is needed for structural failure mode assessment. Simulated static wall pressures overlapped the published HyShot 2 and HDCR pressure ranges and the combustor entrance Mach numbers of 2.4–2.5 were close to both the HyShot 2 combustor entrance value and the HDCR Mach 6 facility nozzle exit value of Mach 2.55. Further, the flow accelerated to Mach 3.3–3.4 through the test modules, as shown in Figure 7.

Peak predicted wall heat flux at the combustor entrance reached 7.1 MW/m^2 in the nominal case and 5.1 MW/m^2 in the lean case, exceeding the 4.2 MW/m^2 recorded by the uncoated, water-cooled

Table 5 – Comparison with reference data from the HyShot 2 flight test, the HDCR ground test, and HIFiRE Flight 2 [17, 18, 24–27]. The HDCR ground test and HIFiRE Flight 2 are listed separately as different test articles in different environments.

	HyShot 2 flight [i]	HDCR ground test (Mach 6 nozzle)	HIFiRE Flight 2	This work (30 s hot-fire)	
				Nominal	Lean
Test duration (s)	3	∼6–10 [a]	9.8 [b]	30	30
Peak wall heat flux (MW/m^2)	not reported	4.2 [c]	not reported	7.1 [d]	5.1 [d]
Static wall pressure (kPa)	60–280	∼90–325 [e]	∼55–620 (predicted) [j]	66–295 [d]	57–250 [d]
Combustor entrance Mach number	M 2.4	M 2.55 [f]	M 2.75–3.65 (predicted) [j]	M 2.4–2.5 [d]	M 2.4–2.5 [d]
Core flow area (cm^2)	7.35	25.8→ 49.2 [g]	as HDCR	52.8	52.8
Test article wall	copper [i]	50 mm copper with 0.6 mm zirconia coating [g]	uncooled, material not reported	C/C liner	
Peak wall temperature (K)	∼350	∼1200 (coating), ∼560 (copper) [h]	not reported	>1500 (thermocouple limit)	

[a] Estimated from Hass et al. [18], Figure 6.
[b] Jackson et al. [26], Table 4: fuelling from 3.22 to 13.0 s.
[c] Hass et al. [18], Figure 20; uncoated, water-cooled gauge.
[d] RANS simulations of this work, 300 K wall boundary condition.
[e] Hass et al. [18], Figure 12 (13–47 psia).
[f] Mach 6 facility nozzle exit, simulating flight Mach 5.84; Hass et al. [18], Table 1.
[g] Hass et al. [18]: flow path 4.0 in wide, 1.0 → 1.908 in high, walls 2.0 in copper with 0.025 in coating.
[h] Coating: Cuda and Hass [27]. Copper: Hass et al. [18], Figure 21.
[i] Smart et al. [24]: 3 s test window, Table 3 windward entrance Mach, 9.8 × 75 mm duct, 350 K wall, copper alloy. Static wall pressure read from Figures 23–25 of Boyce et al. [25].
[j] Storch et al. [17], Figure 10: pre-flight CFD predictions at the isolator entrance over the Mach 6–8 trajectory.

gauge in the HDCR ground test. Since both measurements are cold wall values, the comparison is consistent. This suggests the test provides conservative thermal loading for structural screening.
Despite aerothermal load agreement, the species composition differs substantially between the test and reference cases. The HIFiRE-2 stoichiometric combustion composition was 72.2% N_2, 14.8% H_2O, 12.0% CO_2, and 0.9% Ar by mass [28], whereas the nominal test case contained 63.0% H_2O and 31.7% CO_2, while the lean case contained 65.8% H_2O and 33.0% CO_2, with trace O_2 and OH. H_2O and CO_2 are oxidising species that contribute to erosion and structural failure in composite materials; however, it is unclear if a test containing greater mass fractions of these species would be more or less conservative than flight conditions. Furthermore, because combustion was not modelled in the test article, no additional intermediate species were generated within the combustor. Reacting flow would produce oxidising radicals such as OH and O, contributing to structural and material changes depending on their relative mass fractions and temperatures.
Particulate content is a further limitation because it may add a mechanical erosion component that is not normally present in a scramjet engine flow path. Particulate was visible in the exhaust plume, with greater particulate observed during the lean firing. Large debris was unlikely to dominate the internal erosion response, but smaller particulate may have contributed to mechanical erosion at the wall. The measured erosion should therefore be interpreted as a combined response to thermal loading, oxidising species, local flow structure, material configuration, and possible particulate impact from this test campaign and not a prediction of the material response in flight.

3.4 Role in a Scramjet Structural Test Campaign

Aircraft structural testing is normally staged, rather than taken directly from a design concept to full-scale flight testing. This building block approach is widely used in composite structural testing and verification, where simple specimens first characterise materials before progressively more representative subcomponent, component, and full scale tests validate simulations and identify failure modes [23, 29]. The same approach can be applied to scramjet structural testing. Unit and coupon tests screen candidate materials and characterise them for simulations. Impulse facilities and simu-

lations assess combustion physics. Direct-connect tests expose representative hardware to coupled loading and duration effects before committing to flight testing, which is generally not as repeatable. In this framework, the hybrid rocket direct-connect method sits as an intermediate fidelity step in a broader scramjet structural test campaign, as shown in Figure 11.

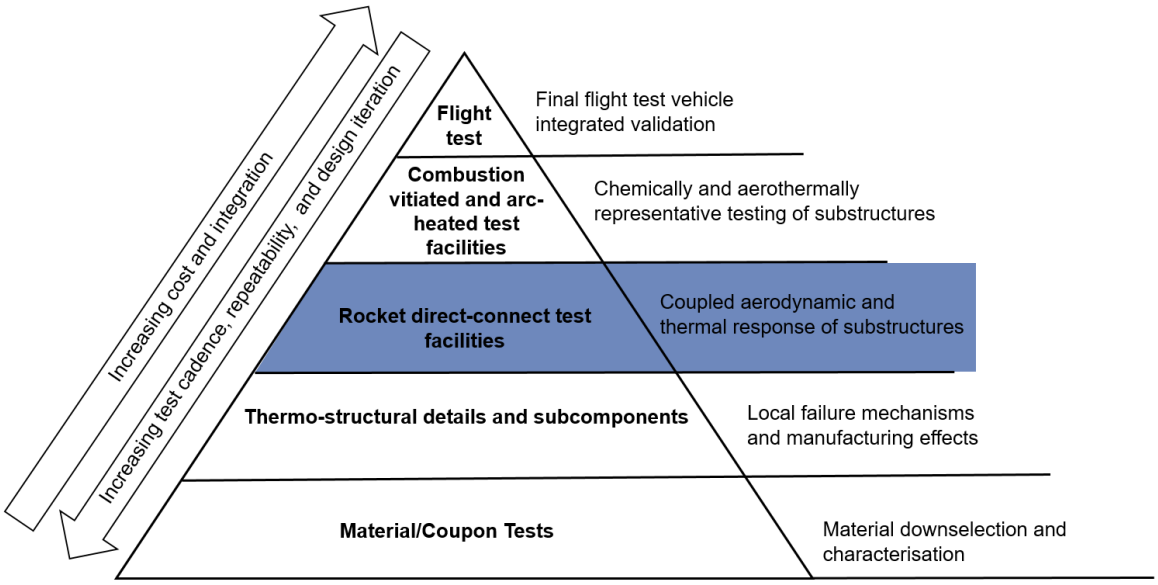


Figure 11 – Building block framework for scramjet thermo-structural verification. The hybrid rocket direct-connect method investigated in this work is an intermediate fidelity full-scale component test.

The method is proposed for screening scramjet engine structures before full system integration. After downselecting materials using unit tests and low fidelity modelling and simulation, a representative duct and nozzle may be built from the selected materials and tested on a hybrid rocket engine test stand. If necessary, several iterations could then be made to improve the original design, at lower cost and a faster pace than international facility access allows. Once confidence is gained in a structure, the engine can proceed to resource-intensive tests such as arc-heated facilities or full flight tests.
Impulse test facilities are not shown in Figure 11 because they support combustion performance prediction and simulation validation rather than structural assessment. This method models the combustor and nozzle only, so it must be supplemented by tests representing the inlet and isolator, and it cannot be used to assess inlet starting, fuel-air mixing, combustion performance, or chemically accurate material recession.

4. Conclusion

This study evaluates the validity of using a hybrid rocket engine as a hot-gas driver for direct-connect thermo-structural screening of scramjet combustor and nozzle structures. Two 30 s hot-fire tests were conducted and simulated, giving static wall pressures of 57–295 kPa, combustor entrance Mach numbers of 2.4–2.5, and peak predicted wall heat flux of 7.1 MW/m^2. These values are consistent with published pressure and combustor entrance Mach number ranges for the HyShot 2 flight and HIFiRE-2 direct-connect ground test reference cases, while providing a longer duration exposure to a representative aerothermal environment than the reference tests.
The coupled experimental and numerical workflow reproduced the dominant pressure, temperature, and shock structure trends sufficiently for preliminary thermo-structural assessment; however, the method should be treated as an intermediate fidelity screening tool rather than a fully representative scramjet combustion test. Wall heat flux and Mach number were derived from simulations assessed against measured static wall pressure and temperature data, and local predictions are uncertain near shock-associated gradients and wall interactions. Further, material recession modelling and prediction of structural failure are not covered in this work.
The principal fidelity limitation is the chemical species mismatch between the hybrid rocket exhaust and a hydrocarbon fuelled scramjet. The test environment was dominated by H_2O and CO_2, in

contrast to the N_2 dominated environment of scramjet combustion; the present method is therefore suitable for assessing coupled aerothermal and mechanical loading, rather than chemically accurate material degradation. Future work should assess liquid hydrocarbon or hydrogen hot-gas drivers, controlled oxygen or nitrogen addition, and species sensitivity studies to quantify how changes in gas composition affect flow properties in direct-connect tests.

5. Acknowledgements

The authors thank Dr Suzanna Turk and Dr Chris Wood for their contribution to wall temperature data acquisition during the test campaign, and the wider Defence Science and Technology Group test team for support during test operations.

6. Copyright Statement

The authors confirm that they, and/or their company or organization, hold copyright on all of the original material included in this paper. The authors also confirm that they have obtained permission, from the copyright holder of any third party material included in this paper, to publish it as part of their paper. The authors confirm that they give permission, or have obtained permission from the copyright holder of this paper, for the publication and distribution of this paper as part of the ICAS proceedings or as individual off-prints from the proceedings.

References

[1] S. Ueda, M. Takegoshi, and T. Kouchi. Evaluation of heat-flux on scramjet engine wall in Mach 6 flight condition. In *55th International Astronautical Congress*, Valencia, Spain, 2006.

[2] S. Luo, D. Xu, J. Song, and J. Liu. A review of regenerative cooling technologies for scramjets. *Applied Thermal Engineering*, 190:116754, 2021.

[3] R. Wang, C. Cheng, X. Yang, L. Bai, J. Zhang, J. Fei, and Q. Fu. Ablation behavior of C/C-ZrC-SiC composites under oxyacetylene, plasma, and plasma-solid particle environments: A comparative investigation. *Materials Characterization*, 219:114649, 2025.

[4] J. Huang, L. Zhao, G. Wang, J. Zheng, A. Lin, and H. Huang. Environment-dependent ablation behavior in C/SiC composites: Modeling across combustion gas and air. *Composites Communications*, 57:102483, 2025.

[5] Y. Yang, S. Zhang, L. Yang, W. Luo, H. Ma, L. Jing, and W. Xie. 'Temperature jump' mechanism of silicon carbide based thermal protection material in arc-jet flow. *International Journal of Thermal Sciences*, 202:109064, 2024.

[6] D. E. Gildfind, R. G. Morgan, P. A. Jacobs, and M. McGilvray. Production of high-Mach-number scramjet flow conditions in an expansion tube. *AIAA Journal*, 52(1):162–177, 2014.

[7] R. J. Stalker. Modern developments in hypersonic wind tunnels. *The Aeronautical Journal*, 110(1103):21–39, 2006.

[8] H. Olivier and S. Gu. Operation, capabilities and limitations of existing hypersonic facilities. In *Flow Characterization and Modeling of Hypersonic Wind Tunnels*, Rhode-St-Genèse, Belgium, 2018. North Atlantic Treaty Organization.

[9] Q. Yang, J. Chang, and W. Bao. Relative time scale analysis for pressure propagation during ignition process of a scramjet. *Aerospace Science and Technology*, 39:206–210, 2014.

[10] R. Xue, G. He, X. Wei, C. Hu, X. Tang, and C. Weng. Experimental study on combustion modes of a liquid kerosene fueled RBCC combustor. *Fuel*, 197:433–444, 2017.

[11] W. Xie, Z. Peng, S. Meng, C. Xu, F. Yi, H. Jin, and S. Du. Thermal stress analysis of the FGLCS in hypersonic vehicles: their application to fuel injection struts in scramjets. *Composites Part A: Applied Science and Manufacturing*, 99:157–165, 2017.

[12] Y. Liu, Z. Xia, L. Ma, P. Yang, B. Chen, Y. Feng, Y. Zeng, C. Li, J. Zhang, and Y. Duan. Microstructure and ablation mechanism of C/C-ZrC-SiC composite in the solid scramjet plumes environment. *Materials Characterization*, 198:112754, 2023.

[13] W. D. Deveikis, R. Miserentino, I. Weinstein, and J. L. Shideler. Aerothermal performance and structural integrity of a René 41 thermal protection system at Mach 6.6. Technical Report NASA TN D-7943, NASA, Hampton, VA, 1975.

[14] K. Daryabeigi, J. R. Knutson, and J. G. Sikora. Thermal vacuum facility for testing thermal protection systems. Technical Report NASA TM-2002-211734, NASA, Hampton, VA, 2002.

[15] L. Zhao, Z. Xia, L. Ma, B. Chen, Y. Feng, P. Yang, C. Li, and Y. Duan. Experimental investigation of combustion mode transitions on solid rocket scramjet combustor. *Aerospace Science and Technology*, 130:107945, 2022.

[16] G. Zhao, R. Ran, C. Zhang, A. Fu, Y. Dou, and L. Shi. Experimental study on the operational characteristics of a scramjet engine under pressure-varying inflow conditions. *Aerospace Science and Technology*, 158:109933, 2025.

[17] A. M. Storch, M. Bynum, J. Liu, and M. Gruber. Combustor operability and performance verification for HIFiRE Flight 2. In *17th AIAA International Space Planes and Hypersonic Systems and Technologies Conference*, San Francisco, CA, 2011. AIAA. AIAA Paper 2011-2249.

[18] N. E. Hass, K. F. Cabell, and A. M. Storch. HIFiRE Direct-Connect Rig (HDCR) Phase I ground test results from the NASA Langley Arc-Heated Scramjet Test Facility. In *JANNAF 43rd CS / 31st APS / 25th PSHS Joint Subcommittee Meeting*, La Jolla, CA, December 2009.

[19] G. Geraci, F. Menhorn, X. Huan, C. Safta, Y. Marzouk, H. N. Najm, and M. S. Eldred. Progress in scramjet design optimization under uncertainty using simulations of the HIFiRE direct connect rig. In *AIAA Scitech 2019 Forum*, pages 1–20, Reston, Virginia, 2019. American Institute of Aeronautics and Astronautics.

[20] S. Walker, F. Rodgers, A. Paull, and D. M. Van Wie. HyCAUSE flight test program. In *15th AIAA International Space Planes and Hypersonic Systems and Technologies Conference*, Dayton, Ohio, 2008.

[21] K. Bowcutt, A. Paull, D. Dolvin, and M. Smart. HIFiRE: An international collaboration to advance the science and technology of hypersonic flight. In *28th International Congress of the Aeronautical Sciences*, pages 65–76, Brisbane, QLD, Australia, 2012. International Council of the Aeronautical Sciences.

[22] National Aeronautics and Space Administration. Langley Research Center's scramjet test complex, 2023. Factsheet.

[23] A. Lockley (now A. Roco). Simulation fidelity of a hybrid rocket engine ground test for structural testing of a Mach 6–8 scramjet combustor and nozzle. Bachelor of Engineering (Honours) thesis, The University of Sydney, Sydney, NSW, Australia, 2024.

[24] M. K. Smart, N. E. Hass, and A. Paull. Flight data analysis of the HyShot 2 scramjet flight experiment. *AIAA Journal*, 44(10):2366–2375, 2006. doi:10.2514/1.20661.

[25] R. Boyce, S. Gerard, and A. Paull. The HyShot scramjet flight experiment - flight data and CFD calculations compared. In *12th AIAA International Space Planes and Hypersonic Systems and Technologies*, Norfolk, Virginia, December 2003. American Institute of Aeronautics and Astronautics.

[26] K. R. Jackson, M. R. Gruber, and S. Buccellato. Mach 6–8+ hydrocarbon-fueled scramjet flight experiment: The HIFiRE Flight 2 project. *Journal of Propulsion and Power*, 31(1):36–53, 2015. doi:10.2514/1.B35350.

[27] V. Cuda, Jr. and N. E. Hass. Heat flux and wall temperature estimates for the NASA Langley HIFiRE Direct Connect Rig. In *JANNAF 43rd CS / 31st APS / 25th PSHS Joint Subcommittee Meeting*, La Jolla, CA, December 2009.

[28] A. D. Sappey, L. Sutherland, D. Owenby, P. VanHoudt, J. Hannam, Q. Zhao, P. J. McCormick, B. P. Masterson, and M. Estes. Flight-ready TDLAS combustion sensor for the HIFiRE 2 Hypersonic Research Program. Technical Report ZD-2231, Zolo Technologies, Boulder, CO, 2009.

[29] Federal Aviation Administration. Composite aircraft structure. Technical Report Advisory Circular AC 20-107B, 2009.